Splitting of Whispering Gallery Modes by Nanoparticles Embedded in High *Q* Microcavities

Kirankumar R. Hiremath, Vasily N. Astratov*

Department of Mathematics, Institute for Scientific Computing and Mathematical Modeling, University of Karlsruhe, Karlsruhe, Germany
e-mail: hiremath@math.uni-karlsruhe.de

**Department of Physics and Optical Science, Center for Optoelectronics and Optical Communications, University of North Carolina at Charlotte, NC, USA*
e-mail: astratov@uncc.edu

ABSTRACT

Effects of perturbations of the whispering gallery modes (WGMs) in cylindrical microcavity resonators by embedded nano size particles are studied by the finite difference time domain modeling. Apart from the foreseeable effects of spectral shift and broadening of WGM resonances, we also observed a key feature of splitting of the WGM peaks. This splitting occurs as a result of formation of symmetric and antisymmetric standing waves inside the cavity. It is demonstrated that magnitude of the splitting reaches several angstroms for 5 μm cavities with index 1.59 supporting moderately high quality ($Q \approx 10^5$) WGMs. We show that this effect allows developing biomolecular sensors based on measuring this splitting in porous cavities or in cavities with liquid cores.

Keywords: resonators, optical confinement, sensors, whispering gallery modes, optics at surfaces, particles scattering

1. INTRODUCTION

Due to high quality (Q) factors of whispering gallery modes (WGMs) in spherical, cylindrical or toroidal cavities they are widely used [1-3] in lab-on-chip and sensor applications. In such cavities WGMs circulate thousands of times inside the cavity that increases their interaction length with the nanoparticles such as DNA, molecules, colloidal particles, or quantum dots located in the vicinity of resonators' surface. The conventional spectroscopic sensors operate based on measurements of a spectral shift or broadening of the corresponding WGM resonance.

One of particularly interesting effects reported for ultra-high Q microspheres [4, 5] and disks [6, 7] is connected with lifting of the degeneracy of counterpropagating (clockwise and anticlockwise) WGMs caused by perturbation near the surface. The magnitude of such observed splitting was rather small, typically in the picometer range with respect to the visible or near infrared wavelengths in these experiments.

In this work we show by using numerical modeling that the sensor devices can be built on a principle based on measurements of a fine splitting of the WGM peaks caused by the embedded nanoparticles. We show that by placing the nanoparticle in an optimal position inside the cavity [8] the WGM splitting can be increased by several orders of magnitude compared to the previously studied case [4-7] of surface perturbations. It is demonstrated that magnitude of the splitting reaches several angstroms for 5 μm cavities with index 1.59 supporting moderately high quality ($Q \approx 10^5$) WGMs. Such splitting is measurable by standard spectrometers. We study the dependence of the magnitude of the splitting on the location, refractive index and size of the embedded nanoparticles. In comparison with conventional spectroscopic sensor devices based on measurements of the WGM spectral shift or broadening effects the proposed devices are expected to be less sensitive to the local heating effects and to the environmental factors that give them a significant performance advantage in real applications. The structures required for realization of this concept include microdroplets with nanometric inclusions, liquid core cylindrical cavities which can be integrated with a microfluidic chip and porous materials.

2. EFFECT OF POSITION OF NANOPARTICLE ON PERTURBATION

We studied the WGM perturbation effects for a two-dimensional (2D) model system, as illustrated in Fig. 1a, consisting of a 5 μm microcylinder supporting WGMs with moderately high $Q \approx 1.4\times10^5$ and an embedded 100 nm nanocylinder with various indices of refraction and radii. This setting is modeled with the standard finite difference time domain method [8]. A built-in source of light launches plane waves at a grazing angle of incidence inside the cavity, as shown in Fig. 1a. Total internal reflection of light leads to formation of WGMs inside the cavity. The position of the monitor where the field is measured along with the position of the embedded nanocylinder is indicated in Fig. 1a. First we consider WGM perturbations as a function of the position of the nanocylinder. The spectra in Fig. 1b and Fig. 1c illustrate the effects of WGM perturbation by the nanocylinder located at various depths d.

978-1-4244-4826-5/09/$25.00 ©2009 IEEE

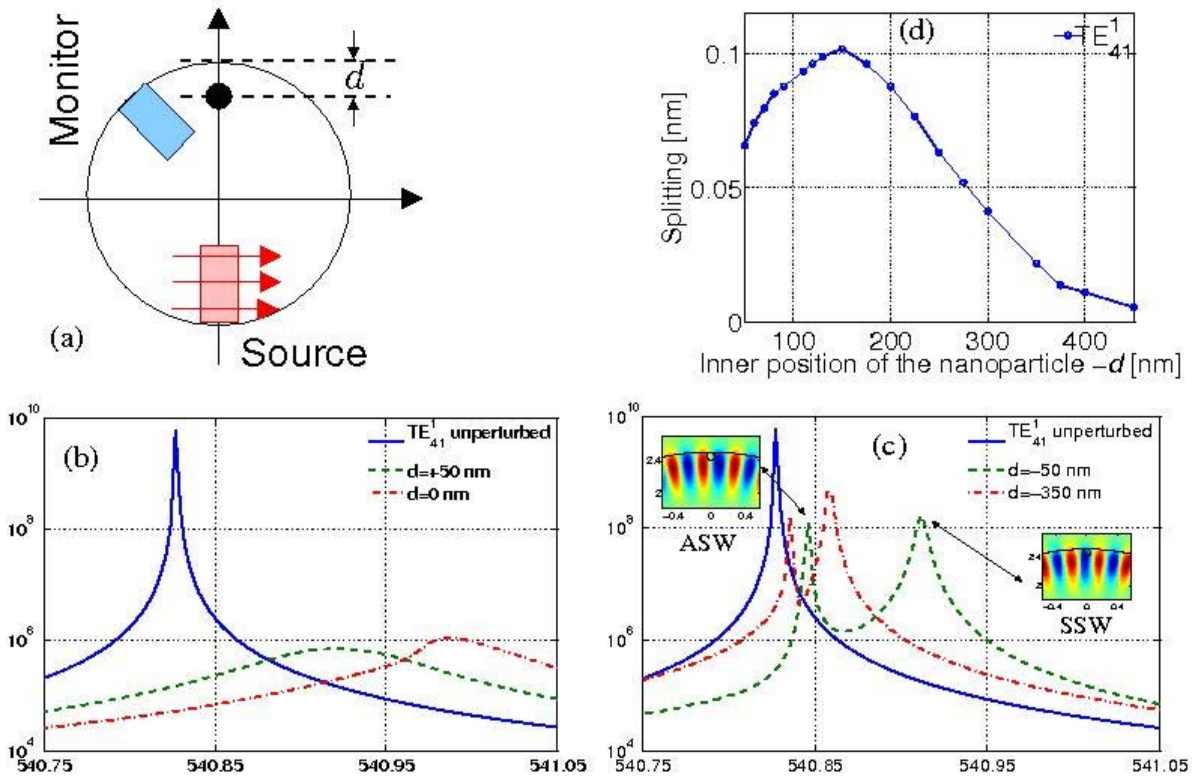

Figure 1. (a) Schematic of the model of cylindrical cavity with nanocylinder perturbation. Figure shows cavity with the built-in source of light and the monitor where the field is measured. The position d of the perturbing nanocylinder is measured as the distance between the center of the nanocylinder and the upper edge of the cavity ($d < 0$ means the nanocylinder is inside the cavity). (b) Effect of perturbations by the nanocylinder of radius R_p=50 nm and index n_p=1.7 located at different d outside the cavity. (c) Effect of perturbations by the nanocylinder as in (b) at different d inside the cavity. The insets illustrate the difference of intensity distributions for the ASW at 540.846 nm and for the SSW at 540.912 nm in terms of their overlap with the nanocylinder. (d) The dependence of SSW/ASW splitting on the position of nanocylinder represented by d.

When the nanocylinder is outside the microcylinder (d = 50 nm) as in Fig. 1b (dashed line), the main effect is a dramatic broadening of the WGM resonance ($Q \approx 3100$) caused by the scattering losses introduced by the nanocylinder. The shift of the peak by 0.093 nm is determined by the increased effective index experienced by the WGM in microcylinder. Similar effect is obtained for the nanocylinder located at the surface of the cavity (d = 0), as illustrated in Fig. 1b (dash dotted line). In this case, an increased long wavelength shift of the resonance is due to the larger overlap of WGM EM field with the high index nanocylinder (n_p = 1.7). In general, for such external perturbation the broadening effects are significant.

When the nanocylinder is completely embedded in the cavity touching its surface from inside (d = -50 nm) as in Fig. 1c (dashed line), the perturbation manifests itself by a double peak structure, one at 540.846 nm and the second at 540.912 nm. In this case, back reflections caused by the strong perturbation by the embedded nanocylinder lead to the formation of clockwise traveling WGMs. For a closer inspection at these two peaks, we launched longer pulses with the bandwidths comparable to the widths of the spectral peaks, and with the center wavelength resonant with the peak positions. The time evolution of the corresponding intensity maps indicates that the both resonances are standing waves as opposed to the uncoupled traveling TE_{41}^1 WGM at 540.83 nm in Fig. 1c (solid line). For a peak at 540.846 nm the overlap of intensity pattern with the nanocylinder is minimized (left inset in Fig. 1c), since the intensity has a zero at the center of nanocylinder. We call this state the asymmetric standing wave (ASW). Due to presence of the node, the ASW not only have the shorter wavelength but also this wave does not effectively interact with the nanocylinder. It results in nearly the same Q-factor ($\approx 10^5$) of this peak as in the reference structure illustrated in Fig. 1c (solid line). In contrast, the peak at 540.912 nm has a maximum at the center of nanoparticle (Fig. 1c right inset). We call this state the symmetric standing wave (SSW). It has a smaller Q-factor ($\approx 10^4$) and it is located at a longer wavelength compared to ASW.

If the nanoparticle is placed deeper (d = -150 nm) inside the cavity, the resulting perturbation of the WGM increases. But when the particle moves in the cavity deeper than the antinode of the radial intensity distribution of TE_{41}^1, the WGM perturbation is reduced, as illustrated by smaller SSW/ASW splitting at d = -350 nm in Fig. 1c (dash dotted line). The plot in Fig. 1d shows in detail this dependence of the splitting on the radial

position of the nanoparticle. It is seen that for the setting under consideration the maximal SSW/ASW splitting is achieved for nanocylinder located at the radial antinode of WGMs at d = 150 nm.

3. EFFECT OF INDEX CONTRAST ON PERTURBATION

Now we investigate influence of the index contrast $\Delta n_p = n_p - n_c$ on the magnitude of splitting of the TE_{41}^{1} resonance peak into SSW and ASW peaks. The absolute positions of the peaks relative to the unperturbed TE_{41}^{1} peak are determined by the average index experienced by the corresponding waves [8]. The ASW peak is found to be shifting only slightly with Δn_p. Due to the small overlap of ASW with the nanocylinder, the corresponding peak was also found to have almost the same $Q \approx 10^5$ in a very broad range of index contrasts, $-0.6 < \Delta n_p < 0.6$, as illustrated in Fig. 2. In contrast, SSW has maximal overlap with the nanocylinder that results in very strong shift of this peak along with pronounced decay of Q-factor with changes in Δn_p.

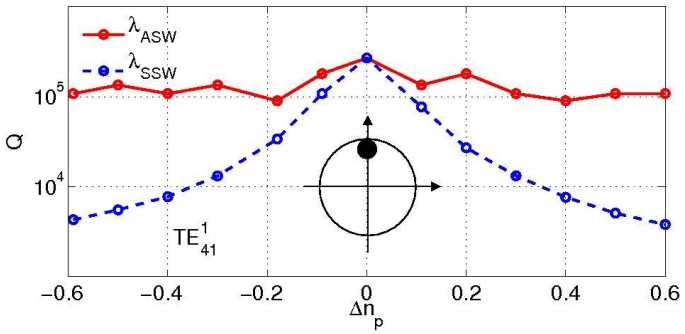

Figure 2. Dependence of the quality factor on the index contrast Δn_p of the perturbation. In these calculations we fix the position of the nanocylinder at $d=-R_p=-50$ nm. Rest of the configuration is same as that for Fig. 1.

It is also found that the splitting $|\lambda_{SSW} - \lambda_{ASW}|$ behaves linearly in the limit of small contrasts. For larger Δn_p (e.g. in the present case for $|\Delta n_p| > 0.2$) however the splitting displays a nonlinear behavior that indicates that such a particle can no longer be considered as a small perturbation [8].

4. EFFECT OF SIZE OF NANOCYLINDER ON PERTURBATION

If the size of the nanoparticle is larger than the wavelength in the medium, then the behavior of ASW resonances should be very different due to the fact that the field can become quite significant at the edges of the particle despite that it has a null at the center of the particle. Such a configuration is simulated with the nanocylinder with index $n_p = 1.64$ placed at $d = -R_p$. The dependence of the SSW and ASW peak positions on R_p is presented in Fig. 3 for a WGM originating from TE_{41}^{1} resonances. It can be seen that in the limit of small sizes ($R_p \leq 50$ nm), as expected, the curve with square marks in Fig. 3 representing the ASW peak shows nearly the same wavelength (= 540.83 nm = resonance wavelength of the unperturbed TE_{41}^{1}), however for larger particles it shows an increasing long wavelength shift. It is interesting to note that for particles with $R_p > 80$ nm the slope of the curve for ASW exceeds that of for the SSW curve (with round marks) which leads to the crossing of these curves around $R_p = 105$ nm. The splitting $|\lambda_{SSW} - \lambda_{ASW}|$ shows pronounced minima around $R_p = 105$ nm, where both SSW and ASW EM field have the same degree of overlap with the embedded particle. The behavior of the curves in Fig. 3 indicates a crossing rather than anticrossing trend around $R_p = 105$ nm.

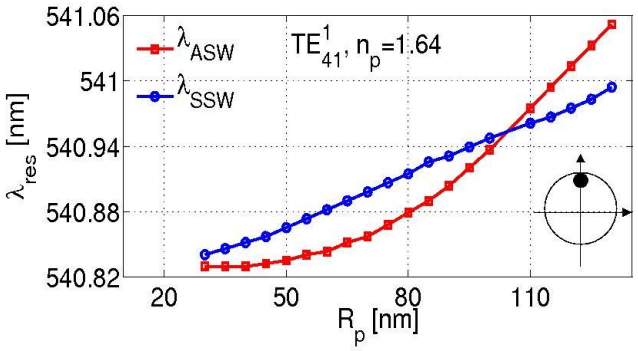

Figure 3. Dependencies of SSW and ASW peak positions on the radius (R_p) of the nanocylinder ($n_p = 1.64$) embedded at $d = -R_p$ deep inside 5 μm microcylinder ($n_c = 1.59$). Rest of the simulation setting is as for Fig. 1.

5. CONCLUSIONS AND OUTLOOK

In this work we showed that by placing the nanoparticle at the antinode of the radial distribution of intensity of WGMs one can obtain SSW/ASW splitting of the order of several angstroms for cavities supporting moderately high quality ($Q \approx 10^5$) WGMs. Such cavities can be realized in various materials systems. The examples include microdroplets with inclusions, liquid core cylindrical cavities which can be integrated with microfluidic chips and permeable or porous materials such as porous silicon [9]. Such splitting effects can be characterized by using conventional spectroscopic tools. We showed that in the limit of relatively small particles ($R_p < 50$ nm) with limited index contrasts ($\Delta n_p < 0.2$) the splitting between SSW and ASW peak is linearly dependent on the size and index of the nanoparticle. This suggests the possibility of developing biomolecular sensors based on the measurement of this splitting. If bacteria, proteins, DNA, and viruses are trapped at an optimal depth inside the cavity, they should produce a certain SSW/ASW splitting which can be used to identify these nano-objects. The values of the splitting determined in this work on the basis of 2D modeling can be used as a rough estimate of the effects which are expected to be observed in such 3D cases.

The results of this work also have a relevance to the case of WGMs in semiconductor microdisks and micropillars with embedded quantum dots (QDs) [10, 11]. On the basis of the present 2D analysis, it is possible to suggest that similar SSW/ASW splitting phenomena can take place in such systems, where self-organized QDs play the part of embedded dielectric particles causing the perturbations. Thus the results of this work can be useful for interpreting spectroscopic studies of high Q semiconductor cavities and photonic molecules with embedded QDs.

ACKNOWLEDGEMENTS

The authors are thankful to S. Arnold for discussions which initiated this work. We also thank M. A. Fiddy for stimulating discussions. This work was supported by NSF under Grant No. ECCS-0824067 as well as, in part, by funds provided by The University of North Carolina at Charlotte. The initial work was supported by ARO Grant W911NF-05-1-0529 (J. T. Prater). K. R. Hiremath acknowledges funding by DARPA Grant No. W911NF-05-2-0053, and also the support by the DFG (German Research Council) Research Training Group 'Analysis, Simulation and Design of Nanotechnological Processes', University of Karlsruhe.

REFERENCES

[1] V. S. Ilchenko and A. B. Matsko, "Optical resonators with whispering gallery modes – Part II: Applications," *IEEE J. Sel. Top. Quantum. Electron*. 12, 15-32 (2006).

[2] R. W. Boyd and J. E. Heebner, "Sensitive disk resonator photonic biosensor," *Appl. Opt*. 40, 5742-5747 (2001).

[3] S. Arnold, M. Khoshsima, I. Teraoka, S. Holler, and F. Vollmer, "Shift of whispering-gallery modes in microspheres by protein adsorption," *Opt. Lett*. 28, 272-274 (2003).

[4] D. S. Weiss, V. Sandoghdar, J. Hare, V. Lefèvre-Seguin, J.-M. Raimond, and S. Haroche, "Splitting of high-Q Mie modes induced by light backscattering in silica microspheres," *Opt. Lett*. 20, 1835-1837 (1995).

[5] T. Kippenberg, S. Spillane, and K. Vahala, "Modal coupling in traveling-wave resonators," *Opt. Lett*. 27, 1669-1671 (2002).

[6] B. E. Little, J. P. Laine, and S. T. Chu, "Surface roughness induced contradirectional coupling in ring and disk resonators*,"* Opt. Lett., 22, 4-6, (1997).

[7] K. Srinivasan, M. Borselli, O. Painter, A. Stintz, and S. Krishna, "Cavity Q, mode volume, and lasing threshold in small diameter AlGaAs microdisks with embedded quantum dots," *Opt. Express* 14, 1094-1105 (2006).

[8] K. R. Hiremath and V. N. Astratov, "Perturbations of whispering gallery modes by nanoparticles embedded in microcavities", *Opt. Express*, 16, 5421-5426 (2008).

[9] L. Pavesi, G. Panzarini, and L. C. Andreani, "All-porous silicon-coupled microcavities: Experiment versus theory," *Phys. Rev. B* 58, 15794-15800 (1998).

[10] E. Peter, P. Senellart, D. Martrou, A. Lemaître, J. Hours, J. M. Gérard, J. Bloch, "Exciton-photon strong-coupling regime for a single quantum dot embedded in a microcavity," *Phys. Rev. Lett*. 95, 067401 (2005).

[11] V. N. Astratov, S. Yang, S. Lam, B. D. Jones, D. Sanvitto, D. M. Whittaker, A. M. Fox, M. S. Skolnick, A. Tahraoui, P. W. Fry, and M. Hopkinson, "Whispering gallery resonances in semiconductor micropillars," *Appl. Phys. Lett*. 91, 071115 (2007).